Peer-reviewed version available at *Materials* **2019**, *12*, 3859; doi:10.3390/ma12233859

Mechanical properties of 3D-printing Polylactic acid parts subjected to bending stress and fatigue testing

J.A. Travieso-Rodriguez[a], R. Jerez-Mesa[b], J. Llumà[c], O. Traver-Ramos[a], G. Gomez-Gras[d], J.J. Roa[c]

[a] Universitat Politècnica de Catalunya, Escola d'Enginyeria de Barcelona Est, Mechanical Engineering Department, Avinguda d'Eduard Maristany, 10-14, 08019 Barcelona, Spain

[b] Universitat de Vic – Universitat Central de Catalunya, Faculty of Sciences and Technology. Engineering Department. C. Laura, 13. 08500 Vic, Spain

[c] Universitat Politècnica de Catalunya, Escola d'Enginyeria de Barcelona Est, Materials Science and Metallurgical Engineering Department, Avinguda d'Eduard Maristany, 10-14, 08019 Barcelona, Spain

[d] IQS School of Engineering. Universitat Ramon Llull, Industrial Engineering Department. Address: Via Augusta, 390. 08017 Barcelona, Spain.

Abstract

This paper aims to analyse the mechanical properties response of polylactic acid (PLA) parts manufactured through fused filament fabrication. The influence of six manufacturing factors (layer height, filament width, fill density, layer orientation, printing velocity, and infill pattern) on the flexural resistance of PLA specimens is studied through an L27 Taguchi experimental array. Different geometries have been tested on a four-point bending machine and on a rotating bending machine. From the first experimental phase, an optimal set of parameters deriving in the highest flexural resistance have been determined. Results show that layer orientation is the most influential parameter, followed by layer height, filament width, and printing velocity, whereas the fill density and infill pattern show no significant influence. Finally, the fatigue fracture behaviour is evaluated and compared with previous studies results, to present a comprehensive study of the mechanical properties of the material under different kind of solicitations.

Keywords: additive manufacturing, 3D printing, fused filament fabrication, flexural properties, fatigue, PLA.

Nomenclature

AM - additive manufacturing

FFF - fused filament fabrication

PLA - polylactic acid

Peer-reviewed version available at *Materials* **2019**, *12*, 3859; doi:10.3390/ma12233859

DOE - design of experiments
ANOVA - analysis of variance

1. Introduction

Manufacturing through Fused Filament Fabrication (FFF) or 3D-printing has been a phenomenon that has changed drastically the way manufacturing is understood mainly during the last decade [1]. The interest comes from the clear advantages that this group of technologies presents with respect to traditional manufacturing technologies: great freedom of design and innovation capacities, a stronger connection between design and manufacturing, or the ability to manufacture unique pieces [2]. In addition, additive manufacturing (AM) systems have been easily implemented in domestic or low-scale manufacturing environments as a cheap and easy manufacturing technology.

Regardless of the rapid expansion of AM, the problem related to the identification and prediction of the mechanical behaviour and physical characteristics of the final pieces has been the main handicap for its application in industrial environments or final pieces. This difficulty lies in the fact that the parameters to be defined during the manufacturing process are numerous and with interactions among them; and, on the other hand, due to the anisotropy of the material, caused by the high influence of the filament orientations in the manufacturing space [3]. Furthermore, anisotropy is also originated due to the difference between the bonding forces between strands of the same layer (intralayer) and between layers (interlayer) [4]. For these reasons, the orientation of the layers is a key parameter to be defined taking into account the work conditions of the piece.

According to Bellehumeur *et al.* [5], the mechanical resistance of parts is the result of the addition of three factors: the resistance of the filaments, the resistance of the union between filaments of the same layer, and the resistance of the union between layers. The inherent resistance of the filaments mainly depends on the mechanical properties of the raw material and the strength of the joints depends on the cohesion between filaments. This is proportional to the thermal energy of the filaments when they come into contact when being placed. The union is a local sinter in which polymer chains are shared. This process is applicable to all joints, between layer threads of both the same layer and different ones.

Authors Gurrala and Regalla [6]; Gray *et al.* [7] and Zhong *et al.* [8] agree that the orientation of the layers must be coincident with the directions of the expected service loads to optimize the mechanical properties. In contrast, in compression forces, due to the buckling effect, the fibres tend to bend. Therefore, the fibres should be oriented perpendicular to the load in this case [9].

Peer-reviewed version available at *Materials* **2019**, *12*, 3859; doi:10.3390/ma12233859

This same effect of the orientation of the layers on the mechanical properties of the workpieces, has also been observed in other processes of AM as in the technology of Laminated Object Manufacturing (LOM), according to Olivier *et al.* [10], selective sintering by laser as reported Ajoku *et al.* [11] or stereolithography presented by Quintana *et al.* [12]

Another parameter with great influence on the mechanical properties is the height of the layer. When the layers have a lower height, the parts show an overall better cohesion between layers, because the contact surface is greater and the empty space between filaments is smaller. This effect improves the transport mechanism of thermal energy favouring the welding between wires as found in Ref. [9]

On the other hand, the thickness or width of the extruded filament is also a parameter that significantly influences the mechanical behaviour. It has a great impact on the transport mechanisms of thermal energy, which will affect the cohesion of the threads, according to the study proposed by Wang [13].

The printing strategy determines the paths of the machine head in the creation of the piece. Within this context, the printed pieces are composed of two characteristic zones: the contour and infill. The outline is the skin that delimits the piece and corresponds to the outer perimeters. Infill is the one formed by the trajectories that the nozzle follows to fill the empty space that remains inside the contour as depicted in Figure 1.

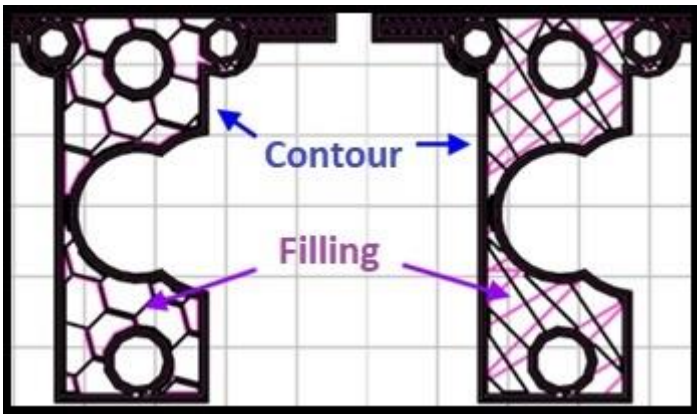

Figure 1. Section of a piece printed with two types of fill patterns. Left: honeycomb, Right: linear.

Generally, in each layer, the contour is first performed and then the internal filling with the selected printing strategy. Each one provides different mechanical properties. In the present work, the influence of several patterns shall be studied, as well as different infill densities, to assess their impact on the workpiece flexural behaviour.

The printing velocity is also a modifiable parameter. It can be defined for each printing zone, being independent for the contours, fills, upper and lower layers. The velocity will be a parameter of study in this work since it has influence in the process of melting and solidification of the filaments. In addition, it affects the rate of extruded material.

Peer-reviewed version available at *Materials* **2019**, *12*, 3859; doi:10.3390/ma12233859

Considering the aforementioned base of knowledge about FFF, this paper aims to study the influence of the manufacturing parameters on the mechanical properties of pieces made of polylactic acid (PLA) manufactured by FFF. Specifically, the flexural mechanical properties of these parts are evaluated. The results obtained are also compared with the ones obtained in a previous by Gómez-Gras *et al.* [17, 18], performed on the same material subjected to a different loading mode. PLA has been scarcely studied in the bibliography, but widely used in the FFF process. For this reason, the results of this study are of great importance for the community of makers, researchers and people in general, who use domestic printers to develop their projects.

2. Materials and Methods

In this paper, the flexural mechanical properties of the PLA have been assessed. The influence of the manufacturing parameters in these properties will also be analysed. Therefore, the first experimental stage explained in this paper comprises a series of four-point bending tests performed on prismatic test specimens, following the ASTM D6272-2 standard [14].

To better understand the influence of the significant parameters, different images of the fractured areas were taken and subsequently analysed. In addition, to complement the fractography a micro scratch test was performed, which helped to better understand the fracture mechanism of the pieces.

In a second experimental stage, a fatigue Whöler curve generated through flexural fatigue tests was drawn to analyse whether the best conditions obtained in the four-point bending tests also derive in good fatigue properties.

2.1 Four-point bending tests

2.1.1 Specimens manufacture

The design of the specimens used in the study was made with Solidworks® software and the models were filleted with Slic3r [15]. Subsequently, they have been manufactured in the domestic 3D printer, Pyramid 3Dstudio XL Single Extruder. Their geometry is shown in Figure 2, dimensions according to the standard that governs the bending test.

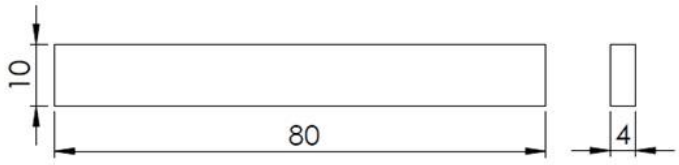

Figure 2. Test specimen's geometry: 80 x 10 x 4 mm, according to the D6272-2 ASTM standard.

The material used in the manufacture of the specimens, as discussed above, is PLA. It is a biodegradable thermoplastic. The choice of PLA as study material is based on the fact that it is the most used material in domestic 3D printing. In this case, the selected filament is manufactured by Fillamentum Company from the Czech Republic. It has a diameter of 3 mm and its extrusion temperature is around 210 ºC. The technical information provided by the manufacturer is indicated in Table 1.

Table 1. Mechanical properties of PLA.

Mechanical property	Value
Yield strength	60 MPa
Elongation at break	6 %
Tensile modulus	3600 MPa
Flexural strength	83 MPa
Flexural modulus	3800 MPa

2.1.2 Taguchi experimental design

To carry out the four-point bending study, the Design of Experiments (DOE) technique was used. The design consists on the combination of the printing parameters that are considered most influential in mechanical behaviour. Six parameters are included in the study, and three levels of each one are defined (Table 2). They have been selected taking into account the bibliography studied, as well as the experience of previous work of the research group.

Table 2. Parameters and levels used in DOE.

Parameter	Level		
	1	2	3
Filament width [mm]	0.3	0.4	0.6
Layer height [mm]	0.1	0.2	0.3
Fill density [%]	25	50	75
Printing velocity [mm/s]	20	30	40
Layer orientation	X	Y	Z
Infill pattern	Linear	Rectilinear	Honeycomb

Preprints (www.preprints.org) | NOT PEER-REVIEWED | Posted: 27 October 2019 doi:10.20944/preprints201910.0293.v1

Peer-reviewed version available at *Materials* **2019**, *12*, 3859; doi:10.3390/ma12233859

Filament width. Determined by the diameters of the extrusion nozzles: 0.3, 0.4 and 0.6 mm. defines the volume and surface of the extruded threads, as well as the welding surface between filaments. (Figure 3 A)

Layer height: Describes the thickness of each layer, and, therefore, the number of layers the printed piece will have. It affects the volume and surface of the threads, as well as in the welding between layers. The manufacturing time is inversely proportional to the layer height. Thinner layers imply more layers to print and more production time. (Figure 3 A)

Fill density: Represents the amount of material that is deposited within the contours. It avoids relative movements between contours and gives robustness to the pieces. It also determines the distance between the inner threads and affects material consumption. (Figure 3 B)

Fill pattern: Defines the trajectories that the nozzle follows to fill the empty space within the contour. Each pattern will create a different interior geometry producing different mechanical behaviours (Figure 3 B).

Orientation: The specimens will be printed in the direction of the 3 coordinate axes: X, Y, and Z, as shown in Figure 4. In this way, the stacking of the layers will be done in three different ways and their behaviour can be studied. Normally, the stacking direction is the most determining factor in mechanical behaviour [16].

Printing velocity: It determines the extrusion and deposition of the threads velocity. The velocity is defined for each part of the piece (inner, external perimeters, inner threads, etc.) to optimize the manufacturing time. In this study, the same velocity is defined for all parts of the piece to homogenize its structure.

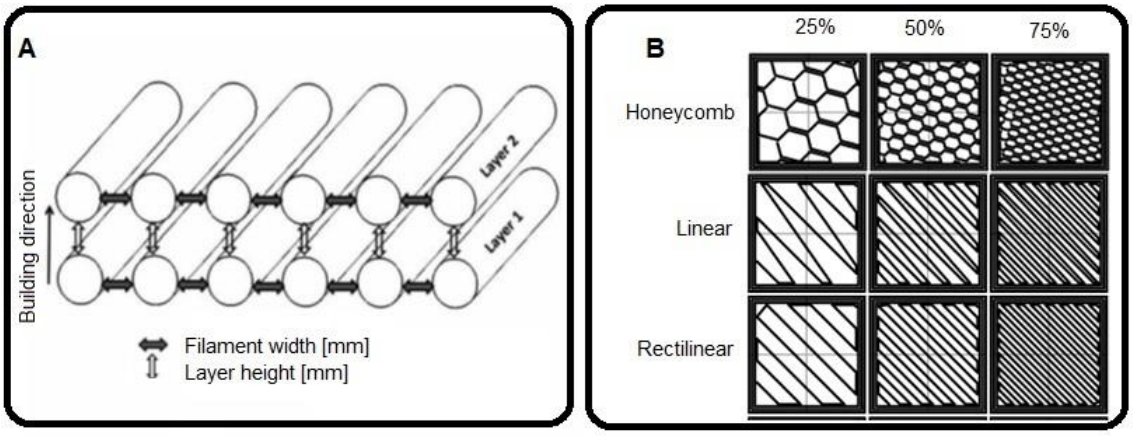

Figure 3. Schematic representation of the parameters used in the study: A- Filament width and Layer height, B- Infill pattern and Fill density.

Preprints (www.preprints.org) | NOT PEER-REVIEWED | Posted: 27 October 2019 doi:10.20944/preprints201910.0293.v1

Peer-reviewed version available at *Materials* **2019**, *12*, 3859; doi:10.3390/ma12233859

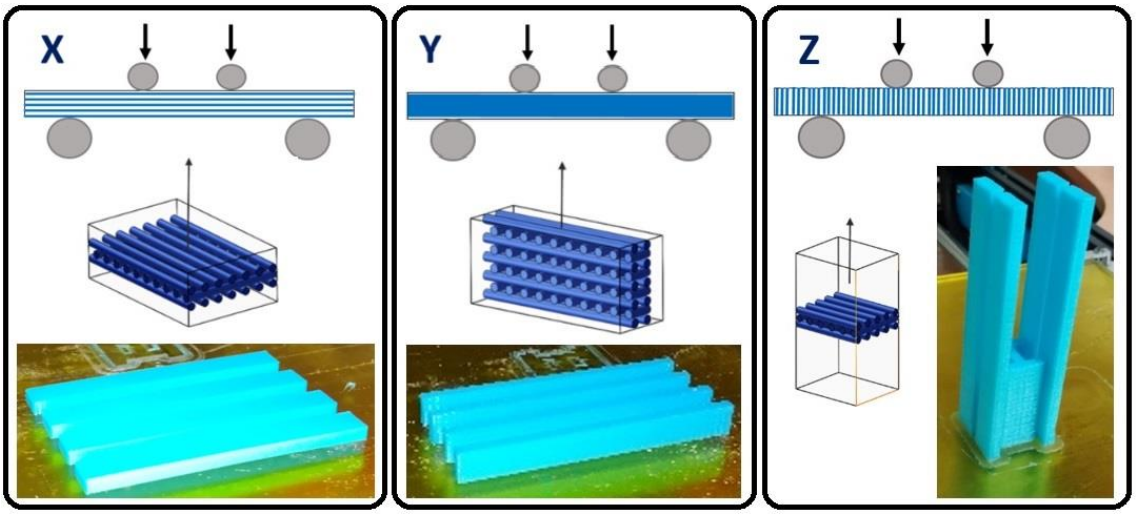

Figure 4. The orientation of the layers stacking, in the manufactured specimens.

In this study, a Taguchi L27 DOE is used. This method has been applied successfully in other studies about the mechanical properties of FFF pieces [17]. Table 3, shows an orthogonal matrix with a specific combination of parameters used. The influence of these separately and their interaction will be studied.

Table 3 Orthogonal matrix of Taguchi L27 for the DOE.

Nº	Filament width [mm]	Layer Height [mm]	Infill density (%)	Printing Velocity [mm/s]	Layer Orientation	Infill
1	0.3	0.1	25	20	X	Rectilinear
2	0.3	0.1	50	30	Y	Linear
3	0.3	0.1	75	40	Z	Honeycomb
4	0.3	0.2	25	30	Y	Honeycomb
5	0.3	0.2	50	40	Z	Rectilinear
6	0.3	0.2	75	20	X	Linear
7	0.3	0.3	25	40	Z	Linear
8	0.3	0.3	50	20	X	Honeycomb
9	0.3	0.3	75	30	Y	Rectilinear
10	0.4	0.1	25	30	Z	Linear
11	0.4	0.1	50	40	X	Honeycomb
12	0.4	0.1	75	20	Y	Rectilinear
13	0.4	0.2	25	40	X	Rectilinear
14	0.4	0.2	50	20	Y	Linear
15	0.4	0.2	75	30	Z	Honeycomb
16	0.4	0.3	25	20	Y	Honeycomb
17	0.4	0.3	50	30	Z	Rectilinear
18	0.4	0.3	75	40	X	Linear
19	0.6	0.1	25	40	Y	Honeycomb
20	0.6	0.1	50	20	Z	Rectilinear
21	0.6	0.1	75	30	X	Linear
22	0.6	0.2	25	20	Z	Linear
23	0.6	0.2	50	30	X	Honeycomb

Preprints (www.preprints.org) | NOT PEER-REVIEWED | Posted: 27 October 2019 doi:10.20944/preprints201910.0293.v1

Peer-reviewed version available at Materials 2019, 12, 3859; doi:10.3390/ma12233859

24	0.6	0.2	75	40	Y	Rectilinear
25	0.6	0.3	25	30	X	Rectilinear
26	0.6	0.3	50	40	Y	Linear
27	0.6	0.3	75	20	Z	Honeycomb

The rest of the parameters that affect the conception of the test specimens remained constant.

2.1.3 Experimental setup

The tests were carried out on the Microtest EM2/20 universal electromechanical machine, with a capacity of 20 kN, displacement of 300 mm, and a speed range 0-160 mm/min. The force acquisition was performed through a load cell of 500 N and a precision of 0.03 N.

The test consists of place the specimen of rectangular cross-section over two supports and load it at two points by means of two loading rollers; each at an equal distance from the adjacent support point. The specimen is bent at a constant speed, until the external fibers break, or until the maximum deformation of the external fibres reaches a 5% elongation. The parameters used in the experiment are described in the D62-72-2 ASTM standard: a support span of 64 mm and a load span of 21.3 mm (Figure 5).

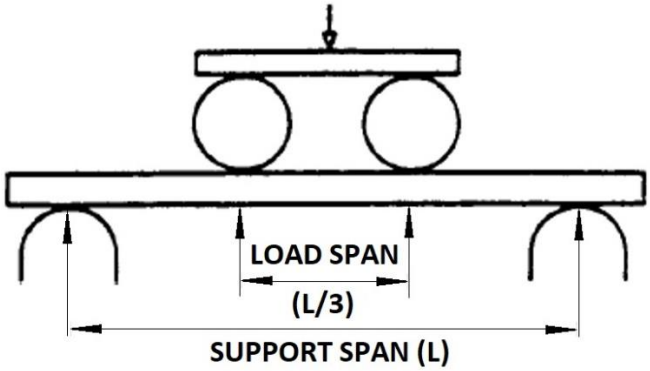

Figure 5. Diagram of the 4 points bending test method, according to the D6272-2 ASTM standard.

The deflection value will be obtained through image processing. High-definition video capture is planned for all tests. That way, the displacement will be obtained through image processing, by following a marker painted on the lower fibre of the specimen. The displacement will be determined to calculate the overall deflection (Figure 6). On the other hand, the force applied by the loading rollers will be measured with a load cell. The objective of data processing is to create the stress-strain curve of the specimens [19]. From the obtained curve, the following results will be extracted: Young's modulus (E), elastic limit ($Rp_{0,2}$), maximum strength (σ_{max}) and maximum elongation (ε).

Preprints (www.preprints.org) | NOT PEER-REVIEWED | Posted: 27 October 2019 doi:10.20944/preprints201910.0293.v1

Peer-reviewed version available at Materials 2019, 12, 3859; doi:10.3390/ma12233859

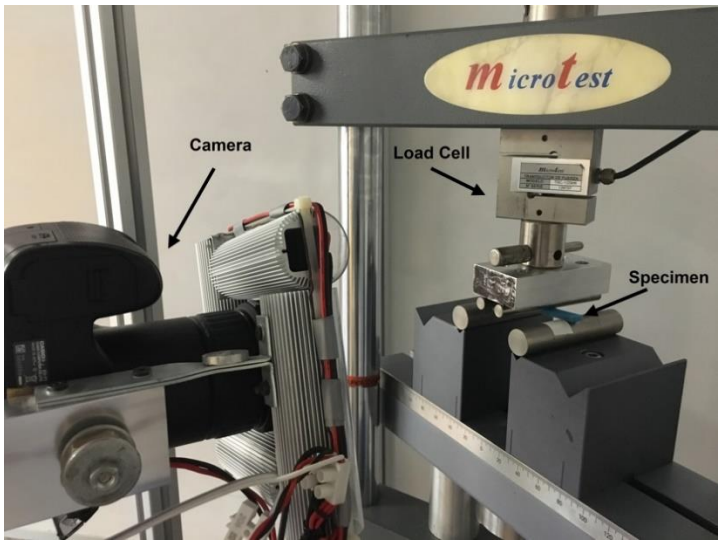

Figure 6. The installation used to perform the 4 points bending tests.

The test method used contemplates two different types, which differ in the test speed according to the behaviour of the test piece.

Type A. Used in test specimens that break with little deflection.

Type B. Used in the test specimens that absorb large deflections during the test.

The Type A test will end when breakage is detected in the outer fibres of the test pieces, and Type B test when the deflection *D* = 10.9 mm, according measurements of the specimens and the parameters used.

A previous experimental testing was performed to validate the adequacy of the described method. From these experiments, it was detected that specimens printed in the direction of the *Z*-axis do not admit deflection, and present brittle failure, while the specimens printed in the direction of the *X* and *Y*-axes admit large deflections. Therefore, the summary of the test types can be seen in Table 4.

Table 4. Test parameters.

Concept	Test type A	Test type B
Specimens orientation	Z	X and Y
Test speed	1.9 mm/min	19 mm/min
End of test	When break appears in the external fibres	When deflection = 10.9 mm

2.1.4 Data analysis

Preprints (www.preprints.org) | NOT PEER-REVIEWED | Posted: 27 October 2019 doi:10.20944/preprints201910.0293.v1

Peer-reviewed version available at Materials 2019, 12, 3859; doi:10.3390/ma12233859

The data analysis was processed by following the steps described as follows:

1. Separation of the frames of the HD videos of each test. The camera used registered the image at 60 fps approximately. The tests lasted between 45 seconds and 2 minutes, so in each of the 108 tests, between 2700 and 7200 frames were processed.
2. Calculation of the specimen's deflection through the frames. Position markers were painted on the outer fibre of the specimen, where the maximum deflection occurs, and on the static rollers (Figure 7 A). The difference of the final position and the initial one, between the most displaced marker of the specimen and the markers on the static rollers, is considered the maximum deflection (Figure 7 B). This analysis was performed through a self-designed MATLAB code with image processing functions.

The calculation of the stress that is generated in the specimen at each moment by means of equation 1:

$$S = \frac{PL}{bd^2} \qquad (1)$$

Where:

S = Stress in the outermost fibre (MPa)

P = Applied load (N)

L = Distance between support rollers (64 mm)

b = Width of the specimen (10 mm)

d = Thickness of the specimen (4 mm)

3. Analysis of the Stress-Strain curve obtained to extract the study parameters.

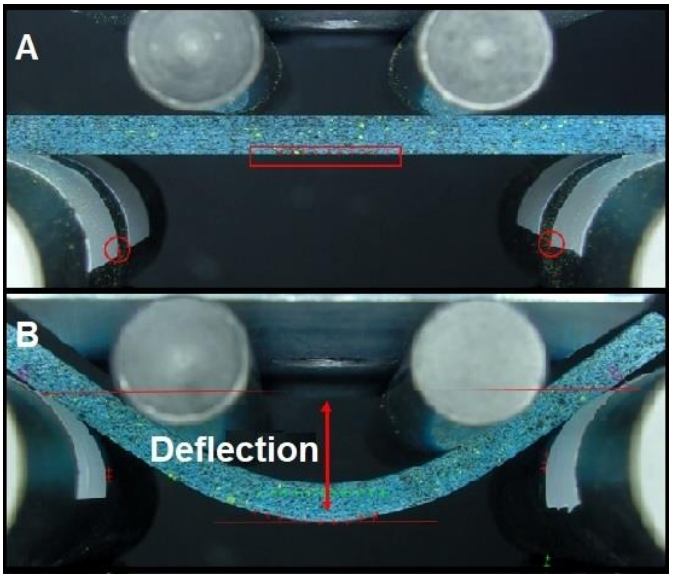

Figure 7. Schematic representation of the data collection process during the tests. A- Initial position of markers, B- Final position (red crosses) and initial (green crosses) of the markers.

Peer-reviewed version available at *Materials* **2019**, *12*, 3859; doi:10.3390/ma12233859

2.2 Fractography and scratch test

In order to analyse the influence of the parameters that have been significant, a SMZ-168 MOTIC stereo microscope was used to observe the fractures surfaces. The most interesting fracture phenomena were photographed with a MOTICAM 2300 camera.

Also, a micro scratch tests were conducted in a Scratch tester unit (CSM-Instruments) using a sphere-conical diamond indenter with a radius of 200 µm. Tests were done under linearly increasing load, from 0 to 70 N, at a loading rate of 10 mm·min^{-1} and in an interval length of 5 mm, according to ASTM C1624-05 Standard [19]. Figures 8 shows the two different scratches per specimen that were carried out in order to observe the reproducibility of the induced damage. Furthermore, the micro scratch tests were conducted in the longitudinal and transversal printing direction to observe the main plastic deformation mechanisms induced. Surface damage induced during scratch tests were observed by a desktop scanning electron microscopy Phenom XL from ThermoFisher Scientific.

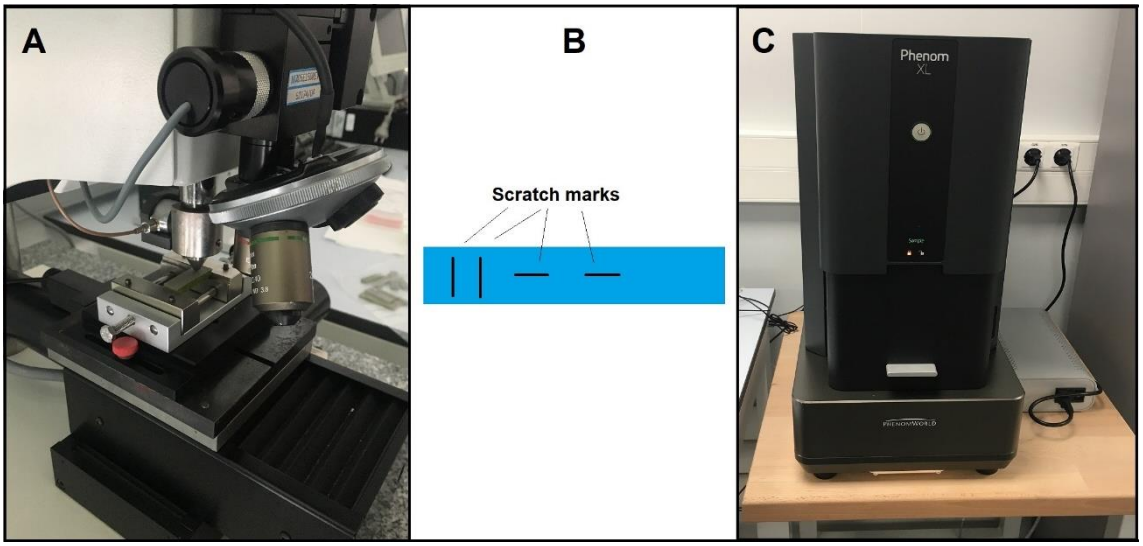

Figure 8. Micro scratch test. A- Scratch tester unit, B- Specimen, C- SEM ThermoFisher Scientific Phenom XL.

2.3 Fatigue test

To complete this study, it is proposed to analyse in a second experimental stage, how cylindrical specimens behave when manufactured through the optimal parameter set found in the previous study, subjected to a rotating fatigue test. This will also allow the comparison with other values previously obtained for the same material using other printing conditions [17].

The rotating bending fatigue test consists on applying a variable bending moment on a cylindrical test piece of known dimensions that rotates on its own axis. In this way, alternative tensile and compressive stresses are generated in the external fibres in each

Preprints (www.preprints.org) | NOT PEER-REVIEWED | Posted: 27 October 2019 doi:10.20944/preprints201910.0293.v1

Peer-reviewed version available at Materials 2019, 12, 3859; doi:10.3390/ma12233859

rotation. The test was carried out on printed cylindrical specimens like the one shown in Figure 9. For the fabrication of the fatigue specimens, the same 3D printer has been used.

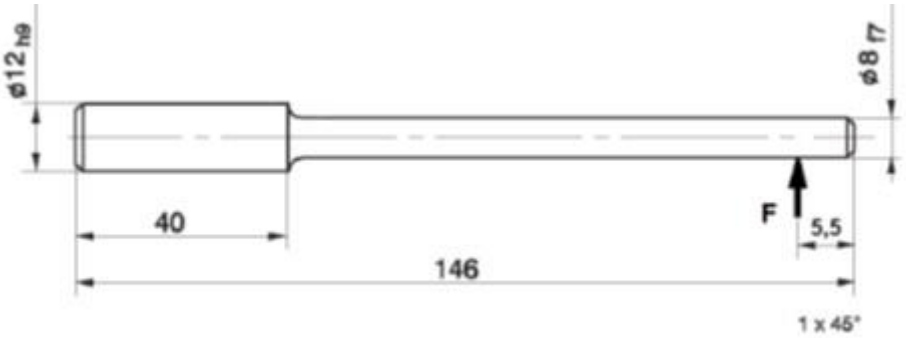

Figure 9. Dimensions of the test specimens used in the fatigue test.

3. Results and discussion

3.1 Four-point bending test

Table 5 shows results, for each printing configuration, of the stress-strain curve as the average results of the five repetitions and their standard deviation.

Table 5. Average results and standard deviations of the material properties.

#	Young's modulus E (GPa)	Standard deviation	Yield strength $Rp_{0,2}$ (MPa)	Standard deviation	Maximum strength σ_{max} (MPa)	Standard deviation	Maximum elongation ε	Standard deviation
1	2.36	0.18	53.8	3.19	64.2	8.18	4.72	1.16
2	3.06	0.07	83.5	0.95	96.0	2.98	4.90	0.64
3	1.79	0.03	11.8	1.74	11.8	1.74	0.70	0.13
4	2.74	0.03	69.7	4.10	79.0	4.97	4.68	1.10
5	1.23	0.10	7.92	1.58	7.96	1.58	0.81	0.24
6	2.71	0.03	60.1	3.09	80.8	2.36	5.85	0.50
7	0.59	0.05	6.71	1.76	6.7	1.76	1.20	0.22
8	2.78	0.11	60.6	3.45	64.1	4.43	3.37	0.32
9	2.81	0.06	65.1	3.61	79.2	6.11	4.91	0.59
10	2.29	0.29	37.1	4.04	37.1	4.04	1.64	0.05
11	3.34	0.19	67.9	3.16	83.7	4.53	4.57	0.17
12	3.69	0.08	95.3	4.26	120.0	1.38	5.34	0.20
13	2.41	0.07	50.2	6.97	72.3	8.23	5.72	0.18
14	3.45	0.33	85.0	3.67	104.6	2.16	4.98	0.17
15	2.07	0.21	26.2	3.34	26.1	3.34	1.49	0.41
16	3.19	0.06	73.4	1.15	83.8	3.87	4.09	0.36
17	1.20	0.09	10.6	1.60	10.6	1.60	1.02	0.13
18	1.44	0.27	26.7	3.25	35.7	4.11	5.09	0.74

Preprints (www.preprints.org) | NOT PEER-REVIEWED | Posted: 27 October 2019 doi:10.20944/preprints201910.0293.v1

Peer-reviewed version available at Materials 2019, 12, 3859; doi:10.3390/ma12233859

19	3.61	0.07	87.4	2.53	95.5	7.35	3.73	0.72
20	3.02	0.27	43.4	3.64	43.5	3.64	1.50	0.12
21	3.23	0.02	70.8	3.51	93.1	4.52	5.09	0.22
22	2.33	0.25	21.3	3.22	21.4	3.22	0.53	0.60
23	2.85	0.19	63.4	6.54	86.4	3.27	5.36	0.64
24	3.70	0.14	90.8	2.28	109.5	4.70	5.11	0.95
25	1.90	0.08	44.0	5.16	60.4	4.43	6.21	0.28
26	2.96	0.15	75.2	3.49	86.7	8.68	4.54	1.56
27	2.30	0.15	25.3	6.61	25.4	6.61	0.91	0.61

An analysis of variance (ANOVA) was performed on the dataset included in the Taguchi experimental array, for each parameter that describes the mechanical behaviour of the evaluated specimens. To validate the statistical relevance of the parameters included in the model, the *p*-value associated with the ANOVA was compared to a significance level of 5%.

One of the first observations derived from the experimental testing, is that specimens printed in the *Z*- direction presented fragile failure, as their failure mode was governed by the lower resistance between layers deposited vertically, thus with a lower neck growth area between them. For that reason, the elastic limit ($Rp_{0,2}$) associated to these specimens was by default considered equal to their maximum strength (σ_{max}). This approach was necessary to perform the statistical analysis, and allows the brittle behaviour to be included in the statistical analysis.

Alongside the yield limit and the maximum strength, the Young's Modulus and maximum elongation were considered as response variables to analyse the influence of the different parameters in the statistical study. The following subsections describe the influence of the different parameters on the considered mechanical properties.

3.1.1 Young's modulus

As a predictable result, the specimens oriented along the *Z*- direction present the lowest rigidity of all, due to their described brittle behaviour, thus can be orientation defined as the most influential parameter (Figure 10 A). The highest deformation module in the elastic regime is defined by an orientation of the fibres along the *Y*- direction, because of the different pattern deposited in this direction with regards to the *X*- orientation

Preprints (www.preprints.org) | NOT PEER-REVIEWED | Posted: 27 October 2019 doi:10.20944/preprints201910.0293.v1

Peer-reviewed version available at *Materials* **2019**, *12*, 3859; doi:10.3390/ma12233859

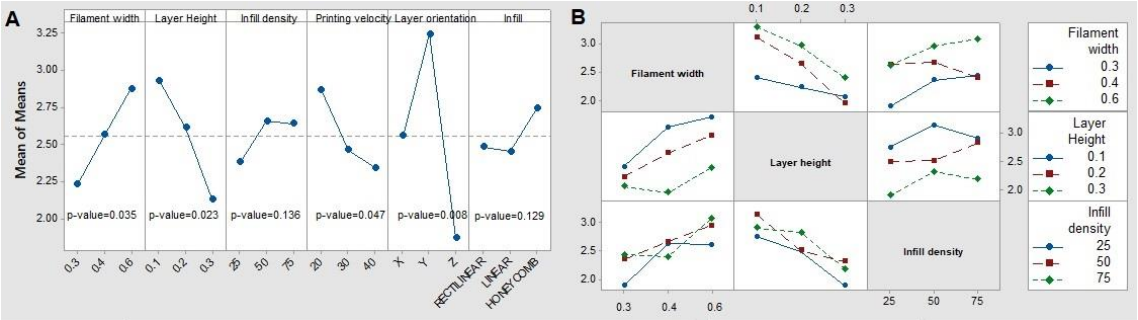

Figure 10. Main effects for A- means and B- interactions, on the Young's Modulus.

On the other hand, an increase in the value of the Young's modulus occurs when the filament width increases, probably because of the higher inertia of the single filaments that restrict bending. This effect of higher inertia of the surface is also achieved by decreasing the layer height, as it derives in a higher value of Young's modulus. This effect could be related to the fact that porosity is decreased by a lower layer height (and complementarily stiffness is increased). Following the same line, the printing velocity proves to increase the stiffness of the specimen as it is lower, probably again by the increase of the overall stiffness.

Of all the tested parameters, both the fill density and the infill pattern have had a negligible impact (*p*-value of the ANOVA test > 5%) and no clear trend, which seems to disagree with the previous analysis. However, it must be considered that the small size of the specimens has derived in a lack of filling, and the geometry was composed basically of boundary layers that have relegated the infill to a second plane in this experimental campaign.

Figure 10 B shows that no significant interaction among parameters is observed, since the *p*-values of them are all greater than 0.05.

3.1.2 Yield strength

Figure 11 shows the influence of the printing parameters on the elastic limit. Again, the layer height and the infill pattern do not show significant influence. The effect of the other parameters on the response follows the same pattern as in the case of Young's modulus. The most influential parameter again is the printing orientation. With the *Y*- orientation, the highest elastic limit is achieved, while with the *Z*- orientation shows the lowest one. In addition, with the *X*- orientation, an intermediate value is achieved with respect to the other printing orientations. The layer height has an influence somewhat higher than that of the filament width, but in the opposite way; as the layer height decreases or the filament width increases, the elastic limit increases. Although the printing velocity has

Preprints (www.preprints.org) | NOT PEER-REVIEWED | Posted: 27 October 2019 doi:10.20944/preprints201910.0293.v1

Peer-reviewed version available at Materials 2019, 12, 3859; doi:10.3390/ma12233859

low relevance, a trend is observed: when the velocity decreases, the elastic limit increases.

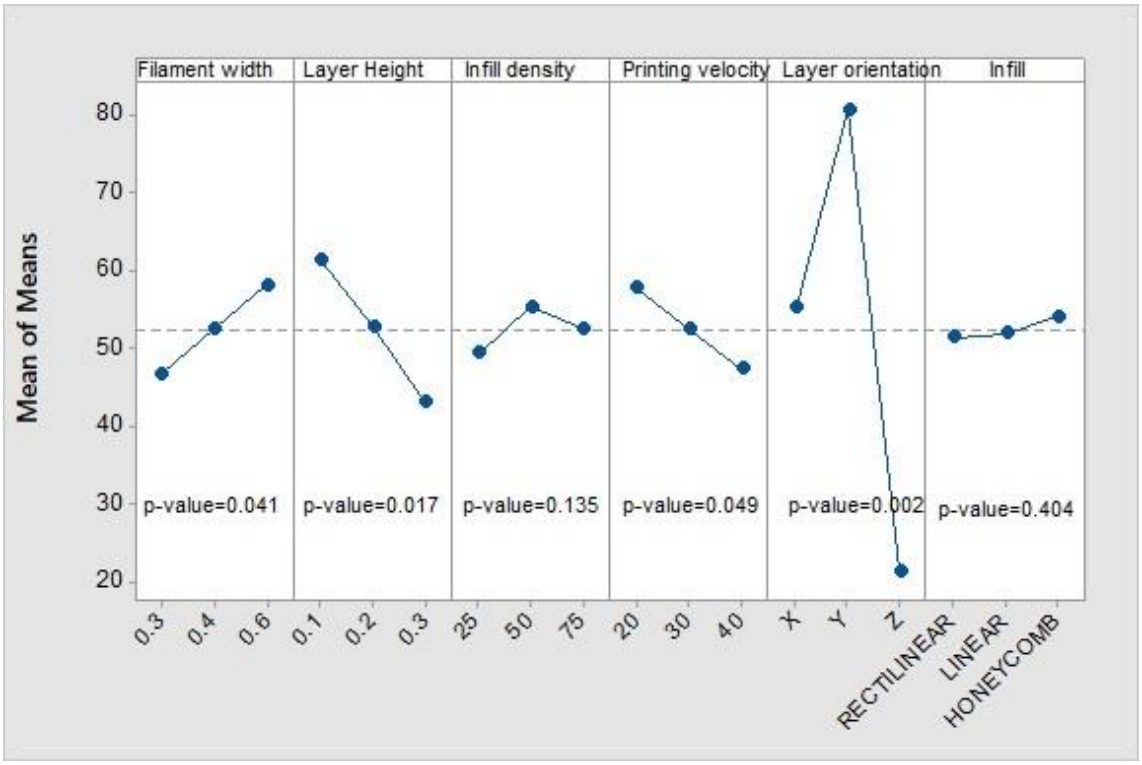

Figure 11. Main effects for means for Yield strength.

When analysing the interactions between the different parameters, it is concluded that there is no significant interaction, since the *p*-values in each case are much higher than 0.05. The same happens for the rest of the parameters. This is positive since it means that the influence of the parameters on the response are independent of each other, at least in the ranges of values analysed.

3.1.3 Maximum strength

The behaviour of the parameters, follow the same pattern as the elastic limit case (Figure 12). The layer orientation is still the parameter with the greatest influence on the means value, followed by the layer height, filament width and printing velocity with less influence. Fill density and infill pattern do not have statistically significant influence.

Preprints (www.preprints.org) | NOT PEER-REVIEWED | Posted: 27 October 2019 doi:10.20944/preprints201910.0293.v1

Peer-reviewed version available at Materials 2019, 12, 3859; doi:10.3390/ma12233859

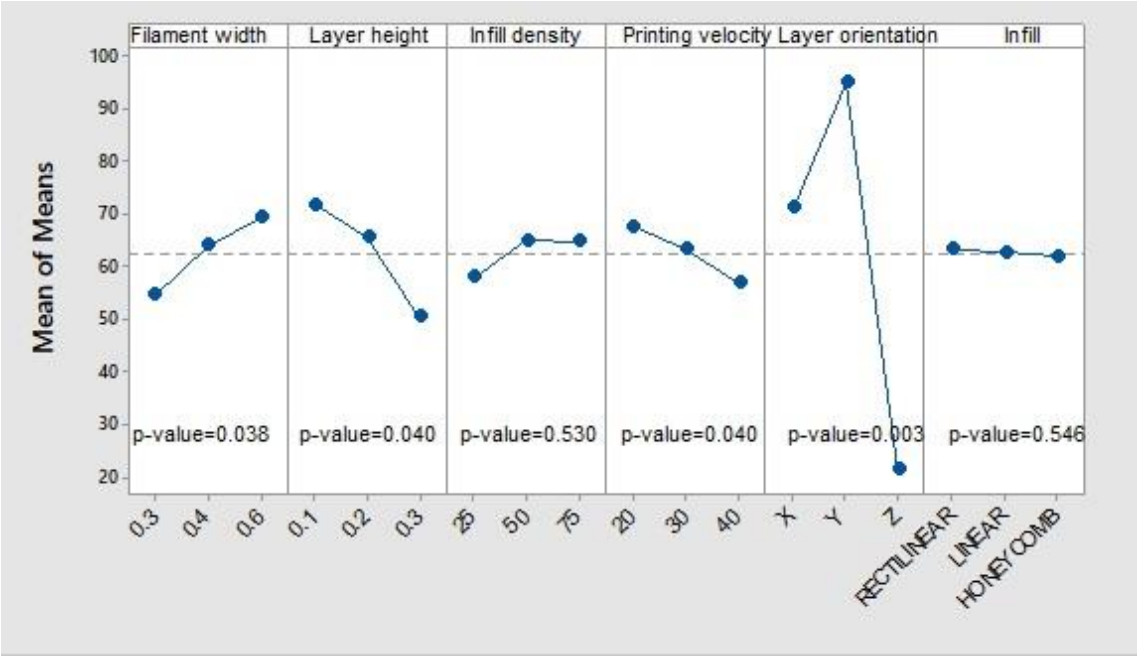

Figure 12. Main effects for means for maximum strength.

3.1.4 Maximum elongation

Figure 13 reveals that the only significant parameter is orientation. The *X*- and *Y*-orientation cause the greatest elongation and the *Z*- orientation, the smallest one. Filament width, layer height, fill density and printing velocity do not present any pattern or proportionality. The Honeycomb fill pattern produces the least effect. Regarding the signal S-N, the only robust parameter is again the orientation.

Preprints (www.preprints.org) | NOT PEER-REVIEWED | Posted: 27 October 2019 doi:10.20944/preprints201910.0293.v1

Peer-reviewed version available at *Materials* **2019**, *12*, 3859; doi:10.3390/ma12233859

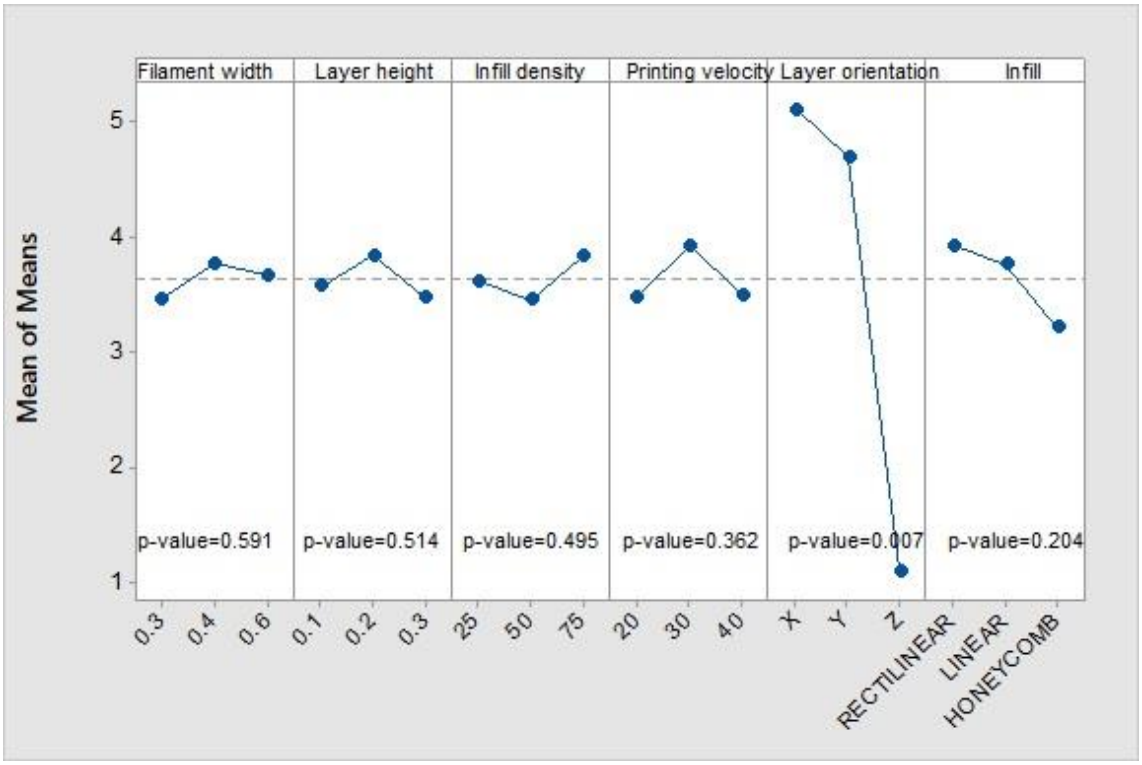

Figure 13. Main effects for means for Maximum elongation.

3.1.5 Summary

In Table 6, a summary of the analysis of the influence of each parameter under study on the different mechanical properties studied can be seen. The orientation is the most influential parameter in both the zone of elastic and plastic behaviour of the pieces tested. The layer height and the filament width are also parameters that influence in all the properties studied, except for the maximum elongation. The same thing happens with printing velocity, but to a lesser extent. In Table 7, the optimum levels of each parameter are shown.

Table 6. Significance value of the parameters with respect to the answers.

Factor	Elastic properties		Plastic properties	
	Young's modulus (E)	Yield strength ($Rp_{0,2}$)	Maximum strength (σ_{max})	Maximum elongation (ε)
Layer orientation	✓ ✓ ✓	✓ ✓ ✓	✓ ✓ ✓	✓ ✓ ✓
Layer Height	✓ ✓	✓ ✓	✓ ✓	✗
Filament width	✓ ✓	✓	✓ ✓	✗

Preprints (www.preprints.org) | NOT PEER-REVIEWED | Posted: 27 October 2019 doi:10.20944/preprints201910.0293.v1

Peer-reviewed version available at Materials 2019, 12, 3859; doi:10.3390/ma12233859

Printing velocity	✓	✓	✓	✗
Infill density	✗	✗	✗	✗
Infill pattern	✗	✗	✗	✗

Table 7. Parameters level to maximize the response.

Factor	Young's Modulus (E)	Yield Strength ($Rp_{0,2}$)	Maximum Tension (σ_{max})	Maximum Elongation (ε)
Filament width	0.6 mm	0.6 mm	0.6 mm	0.2 mm
Layer Height	0.1 mm	0.1 mm	0.1 mm	0.2 mm
Infill density	75%	75%	75%	75%
Printing Velocity	20 mm/s	20 mm/s	20 mm/s	30 mm/s
Layer Orientation	Y	Y	Y	X
Infill pattern	Honeycomb	Honeycomb	Honeycomb	Rectilinear

3.2 Fractography and scratch test

It was already noted that the main factor that determines the strength of the specimens is the orientation of the stacking layers. In figure 14, the outlook of the fracture section of some printed specimens in the different directions of the coordinate axes are compared. The specimens printed along the *X*- direction (Figure 14 A) or along the *Y*- direction (Figure 14 B) have a slight ductile behaviour with high elongation, good flexural strength, and high rigidity. This reaction is caused by the filaments being aligned with the main stress direction. The resistance depends on the strength of the intra-layer bond and the strength of the filaments. The stiffness and flexural strength are slightly higher in the *Y*-orientation specimens. The reason is once again the arrangement of layers. Although the two orientations have the filaments parallel to the direction of the stresses, the specimens printed in the *X*- direction can become delaminated between layers when they are bent. The delamination is produced by the breakage of the weak interlayer bonds. The specimen becomes flexible and is unable to withstand the bending stress, although the intralayer bonds remain intact.

Preprints (www.preprints.org) | NOT PEER-REVIEWED | Posted: 27 October 2019 doi:10.20944/preprints201910.0293.v1

Peer-reviewed version available at Materials 2019, 12, 3859; doi:10.3390/ma12233859

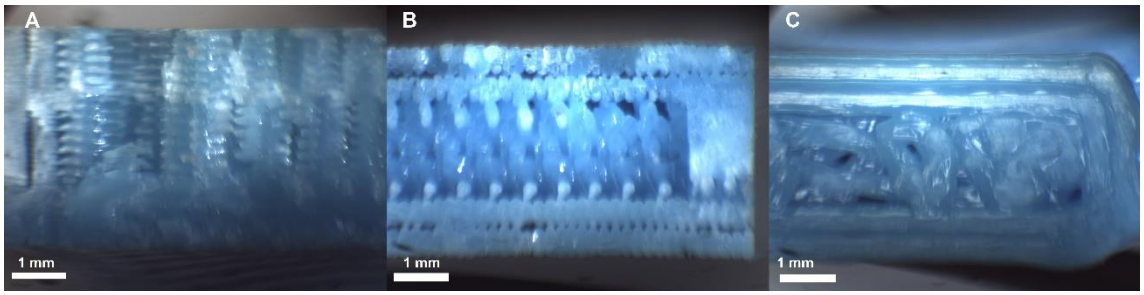

Figure 14. Breaking section, specimens with orientation in A-X, B-Y, C-Z.

In Figure 14 C, the section of the rupture of a test specimen printed in *Z*- orientation is shown. These specimens have fragile behaviour and little deformation, low resistance to bending and low rigidity. This is caused because the layers are oriented perpendicularly to the stresses generated in the specimen during the bending test. For this reason, failure has occurred in the weak interlayer weld without the affection of filament integrity.

The second most influent factor is the layer height, followed by the filament width. The smaller the layer height and the larger the filament width, the stiffer and more resistant to bending has been the test specimen. This is directly related to the compactness of the threads and the welding between threads (Figure 15).

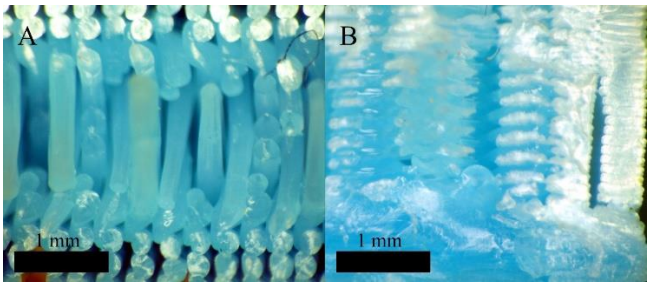

Figure 15. A- Test specimen with a layer height of 0.3 mm and filament width 0.3 mm. Test specimen 9_2. Microscopic photography, B- Test specimen with layer height 0.1 mm and filament width 0.6 mm. Test specimen 21_3. Microscopic photography.

Figure 15 A shows the extreme case with the maximum layer height 0.3 mm and the minimum filament width 0.3 mm. With these dimensions, the threads are cylindrical and produce low compaction and weak welding due to the scarce contact surface between threads. On the other hand, as the layer height decreases and the filament width increases, the threads have a flat shape, with a larger welding surface. Figure 15 B shows the optimal case with a minimum layer height of 0.1 mm and the maximum filament width of 0.6 mm. In summary, the welding surface of the threads, where the micro-welds are produced between the chains of the polymer deposited at the beginning and those of the filament that is then deposited on it, is determinant in the mechanical

Preprints (www.preprints.org) | NOT PEER-REVIEWED | Posted: 27 October 2019 doi:10.20944/preprints201910.0293.v1

Peer-reviewed version available at Materials 2019, 12, 3859; doi:10.3390/ma12233859

behaviour. The greater the welding surface, the greater the rigidity and strength of the piece.

Figure 16 shows the micro scratch test tracks in both A- perpendicular and B- parallel direction to the filaments; on the same piece printed in the X- direction shown in figure 14 A. It can be seen how up to the tested force (70 N), the material deforms ductilely without cracking in the base material, as the indenter moves. It also looks like the burrs produced by the extruder are torn. The fact that there are no disclosures between filaments implies that the adhesion between them in the same layer is enough to resist the efforts applied during the test.

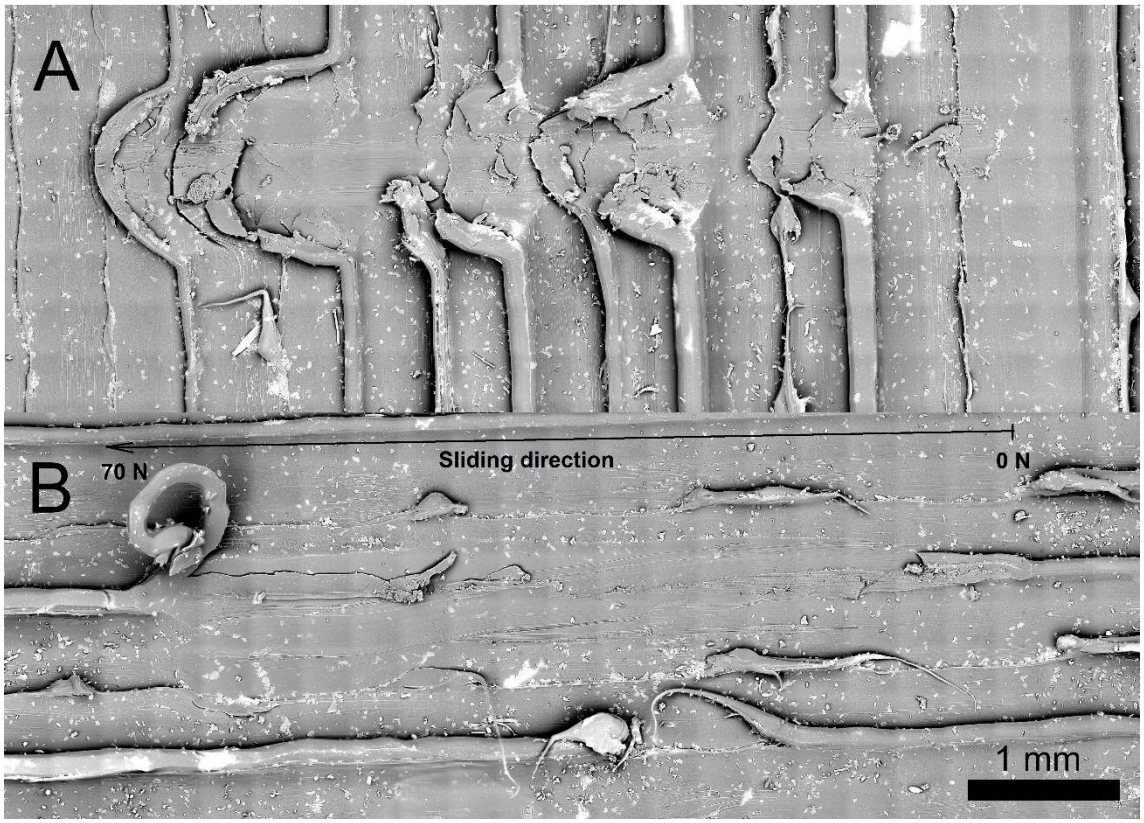

Figure 16. Micro scratch test A- Perpendicular to the printing direction, B- Parallel to the printing direction.

The graph in figure 17 shows the results of the micro-scratch tests: A-perpendicular and B- parallel to the direction of the filaments in the range of test forces. The values of: Normal force, friction force, penetration depth, Residual depth and friction coefficient, are clearly observed. While the value of the friction coefficient measured in the perpendicular test, shows oscillations due to abrasive wear of the burrs (see arrows in figure 17 A), in the parallel test its value remains almost constant. It could be possible to sense that these pieces are not showing wear remarkable adhesive.

On the other hand, these burrs left during the extrusion process, form channels on the piece surface. If it is true that this worsens the surface roughness of the pieces, they

Preprints (www.preprints.org) | NOT PEER-REVIEWED | Posted: 27 October 2019 doi:10.20944/preprints201910.0293.v1

Peer-reviewed version available at Materials 2019, 12, 3859; doi:10.3390/ma12233859

could be useful for retaining lubricant adhered to the sides of the burr ridges; more taking into account that they do not increase their friction coefficient too much, as shown in Figure 17.

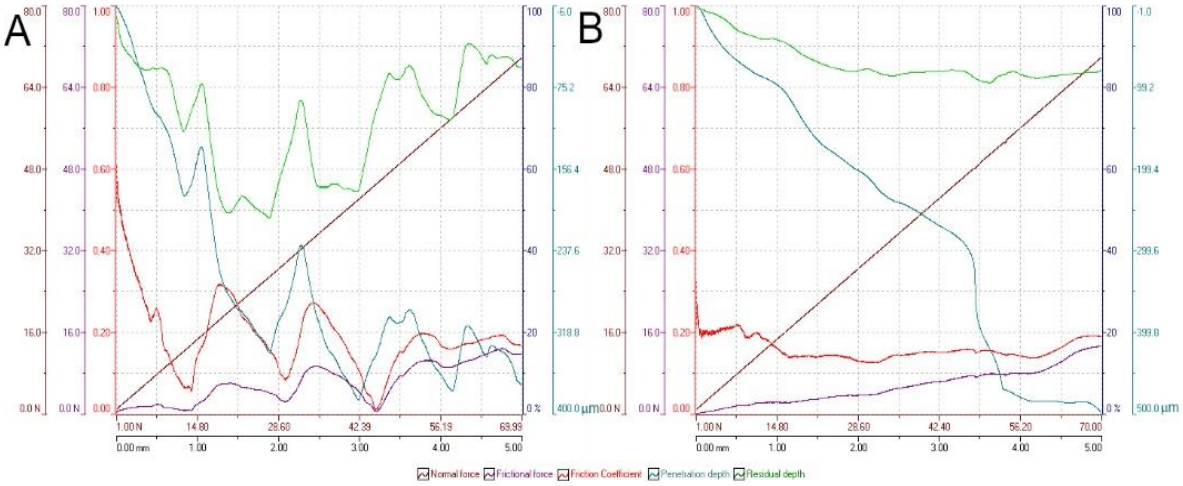

Figure 17. Micro scratch test results A- Perpendicular to the printing direction, B- Parallel to the printing direction

3.3 Fatigue test

The parameter that marks the difference between both curves in Figure 18 is the layer height, being 0.1 mm for the results of this study and 0.3 mm for the referenced study [17].

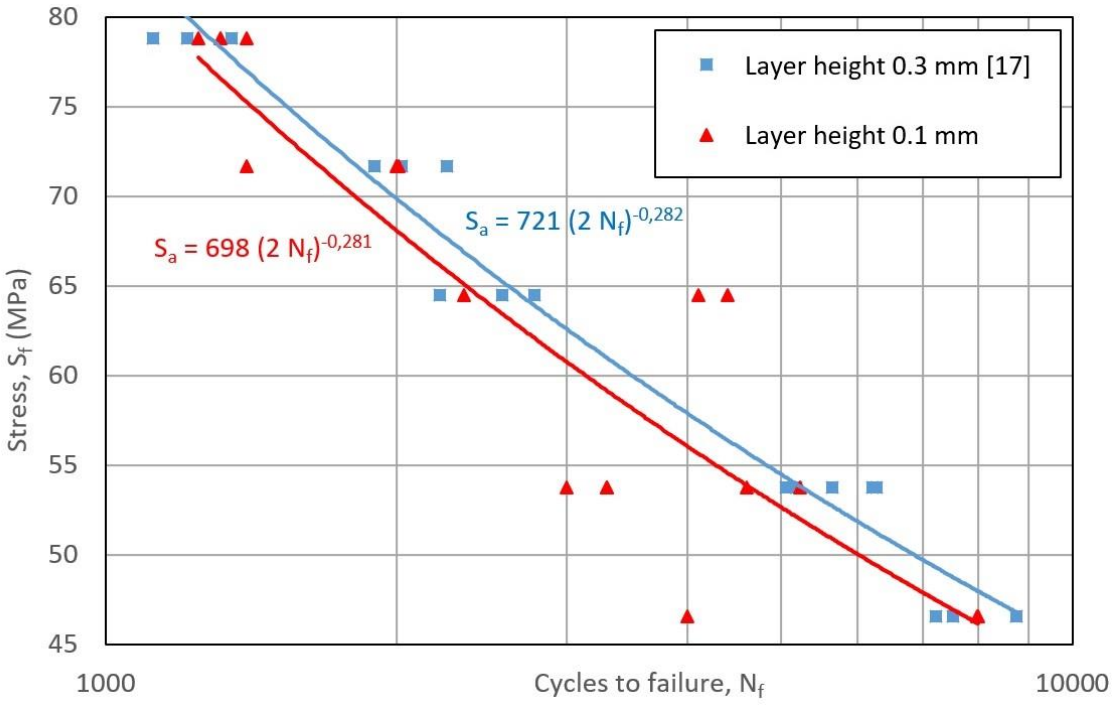

Figure 18. Wöhler curve, for the results obtained in this study and those obtained in [17].

Peer-reviewed version available at *Materials* **2019**, *12*, 3859; doi:10.3390/ma12233859

Although [17] find that layer height is slightly significant, and it seems that there is a relationship between the following assumptions: the higher the height layer value, the more improvement is detected regarding resistance; this cannot be assured, since the errors calculated for the multiplicative factor and the exponent in both equations causes that they can be the same.

Therefore, although a dependence on the layer height is insinuated, the current data does not allow it to assert it.

4. Conclusions

The influence of layer orientation, layer height, filament width, printing velocity, fill density and infill pattern on the flexural performance of PLA specimens has been studied through a Taguchi DOE. The following conclusions can be extracted:

1. The orientation of the stacking of the layers is the most influential parameter in the rigidity, in the flexural resistance, and in the maximum deformation.
2. The layer height and the filament width have had a great significance in stiffness and flexural strength and no influence on maximum deformation.
3. Printing velocity has had a small but significant effect on rigidity and flexural strength and no influence on maximum deformation.
4. The fill density and the infill pattern have had no effect on the studied mechanical properties.
5. The orientation of stacking layers in Y, the layer height of 0.1 mm, the filament width of 0.6 mm and the printing velocity of 20 mm/min, has been the optimal combination obtained that will allow maximizing rigidity and flexural resistance.
6. The printing direction in *Y* has shown the best mechanical behaviour due to its resistance depends on the strong intralayer bond.
7. The large filament width, the small layer height, and the low printing velocity have formed test specimens with better compaction, better welding between wires, generating a better rigidity and resistance to bending.
8. It could not be ensured that higher layer height improve fatigue life.
9. Depending on the mechanical property to enhance, the combination of optimal parameters to use is different.

Data availability

The raw/processed data required to reproduce these findings cannot be shared at this time as the data also forms part of an ongoing study.

Funding

This research did not receive any specific grant from funding agencies in the public, commercial, or not-for-profit sectors.

Acknowledgments

Dr. J.J. Roa would like to acknowledge the Serra Hunter program of the *Generalitat de Catalunya*

References

1. Go, J., Schiffres, S.N., Stevens, A.G., Hart, A.J.: Rate limits of additive manufacturing by fused filament fabrication and guidelines for high-throughput system design. Addit. Manuf. 16, 1-11 (2017)
2. Fontrodona, J., Blanco, R.: Estado Actual y perspectivas de la impresión en 3D. Artículos de Economía Industrial. http://empresa.gencat.cat/web/.content/19_-_industria/documents/economia_industrial/impressio3d_es.pdf (2014). Accessed 4 July 2019
3. Domingo-Espin, M., Puigoriol-Forcada, J.M., Garcia-Granada, A.A., Llumà, J., Borros, S., Reyes, G.: Mechanical property characterization and simulation of fused deposition modeling Polycarbonate parts. Mater Design. 83, 670-677 (2015)
4. Bellini, A., Güçeri, S.: Mechanical characterization of parts fabricated using fused deposition modeling. Rapid Prototyp J. 9 (4), 252-264 (2003)
5. Bellehumeur, C., Li, L., Sun, Q., Gu, P.: Modeling of Bond Formation Between Polymer Filaments in the Fused Deposition Modeling Process. J Manuf Process, 6 (2), 170-178 (2004)
6. Gurrala, P.K., Regalla, S.P.: Part strength evolution with bonding between filaments in fused deposition modelling: This paper studies how coalescence of filaments contributes to the strength of final FDM part. Virtual Phys Prototyp. 9 (3), 141-149 (2014)
7. Gray, R.W., Baird, D.G., Helge Bøhn, J.: Effects of processing conditions on short TLCP fiber reinforced FDM part. Rapid Prototyp J. 4 (1), 14-25 (1998)
8. Zhong, W., Li, F., Zhang, Z., Song, L. and Li, Z.: Short fiber reinforced composites for fused deposition modelling. Mater. Sci. Eng. A. 301 (2), 125-130 (2001)
9. Sood, A.K., Ohdar, R.K., Mahapatra, S.S.: Parametric appraisal of mechanical property of fused deposition modelling processed parts. Mater Design. 31 (1), 287-295 (2010)

10. Olivier, D., Travieso-Rodriguez, J.A., Borros, S., Reyes, G., Jerez-Mesa, R.: Influence of building orientation on the flexural strength of laminated object manufacturing specimens. J Mech Sci Technol. 31 (1), 133-139 (2017)
11. Ajoku, U., Saleh, N., Hopkinson, N., Hague, R., Erasenthiran, P.: Investigating mechanical anisotropy and end-of-vector effect in laser-sintered nylon parts. Proc Inst Mech Eng B J Eng Manuf. 220 (7), 1077-1086 (2006)
12. Quintana, R., Choi, J.W., Puebla, K., Wicker, R.: Effects of build orientation on tensile strength for stereolithography-manufactured ASTM D-638 type I specimens. Int J Adv Manuf Technol. 46 (1), 201-215 (2010)
13. Wang, T., Xi, J. and Jin, Y.: A model research for prototype warp deformation in the FDM process. Int J Adv Manuf Technol. 33 (11), 1087-1096 (2007)
14. ASTM D6272–02, Standard Test Method for Flexural Properties of Unreinforced and Reinforced Plastics and Electrical Insulating Materials by Four-Point Bending. Ed. West Conshohocken, PA, ASTM International (2002)
15. Hodgson, G.: Slic3r Manual - Infill Patterns and Density. Manualslic3rorg. http://manual.slic3r.org/ (2017). Accessed 4 July 2019
16. Puigoriol-Forcada, J.M., Alsina, A., Salazar-Martín, A.G., Gomez-Gras, G., Pérez, M.A.: Flexural Fatigue Properties of Polycarbonate Fused-deposition Modelling Specimens. Mater Design. 141, 414–425 (2018)
17. Gomez-Gras, G., Jerez-Mesa, R., Travieso-Rodriguez, J.A., Lluma-Fuentes, J.: Fatigue performance of fused filament fabrication PLA specimens. Mater Design. 140, 278-285 (2018)
18. Jerez-Mesa, R., J.A., Travieso-Rodriguez, Lluma-Fuentes, J., Gomez-Gras, G., Puig, D., Fatigue lifespan study of PLA parts obtained by additive manufacturing. Procedia Manufacturing, 13 (2017) 872-879.
19. Morales-Planas, S., Minguella-Canela, J., Lluma-Fuentes, J., Travieso-Rodriguez, J.A., García-Granada, A.A.: Multi Jet Fusion PA12 manufacturing parameters for watertightness, strength and tolerances. Materials, 11(8), 1472 (2018)
20. ASTM C1624-05, Standard Test Method for Adhesion Strength and Mechanical Failure Modes of Ceramic Coatings by Quantitative Single Point Scratch Testing. ASTM International Standards, USA (2005)